Journal of the Mechanical Behavior of Biomedical Materials 75 (2017) 549–557

Contents lists available at ScienceDirect

Journal of the Mechanical Behavior of Biomedical Materials

journal homepage: www.elsevier.com/locate/jmbbm

# Mechanical properties of a collagen fibril under simulated degradation

David C. Malaspina[a,b], Igal Szleifer[a], Yasin Dhaher[a,b,*]

[a] Biomedical Engineering Department, Northwestern University, 2145 Sheridan Road, Evanston, IL 60208, USA
[b] Rehabilitation Institute of Chicago, 345 E. Superior, Chicago, IL 60611, USA

ARTICLE INFO

*Keywords:*
Collagen
Molecular dynamics
Degradation
MMP

ABSTRACT

Collagen fibrils are a very important component in most of the connective tissue in humans. An important process associated with several physiological and pathological states is the degradation of collagen. Collagen degradation is usually mediated by enzymatic and non-enzymatic processes. In this work we use molecular dynamics simulations to study the influence of simulated degradation on the mechanical properties of the collagen fibril. We applied tensile stress to the collagen fiber at different stages of degradation. We compared the difference in the fibril mechanical priorities due the removal of enzymatic crosslink, surface degradation and volumetric degradation. As anticipated, our results indicated that, regardless of the degradation scenario, fibril mechanical properties is reduced. The type of degradation mechanism (crosslink, surface or volumetric) expressed differential effect on the change in the fibril stiffness. Our simulation results showed dramatic change in the fibril stiffness with a small amount of degradation. This suggests that the hierarchical structure of the fibril is a key component for the toughness and is very sensitive to changes in the organization of the fibril. The overall results are intended to provide a theoretical framework for the understanding the mechanical behavior of collagen fibrils under degradation.

## 1. Introduction

The molecular structure of collagen is characterized by a hierarchical multi-scale organization that grants high elasticity, large fracture strength and large energy dissipation upon deformation (Fratzl, 2008). The key building block is the tropocollagen molecule formed by a triple helix of three polypeptides chains with a length of ~ 300 nm. Tropocollagen molecules arranged in groups to form more complex structures: micro-fibrils, fibrils and fibers. Micro-fibrils have an approximate diameter of ~ 4 nm and are the minimum structure that presents the characteristic D-banding as a consequence of gaps and overlaps between tropocollagen. These micro-fibrils self-assemble in larger bundles forming collagen fibrils. The approximate length of fibrils is on the order of ~ 1 μm. Finally, bundles of fibrils form higher hierarchy units: the collagen fibers. These fibers are the main constitutive unit of different connective tissues and the approximate length is ~ 10 μm (Hulmes, 2002; Shoulders and Raines, 2009; Prockop and Kivirikko, 1995). In this work we are going to focus on the intermediated hierarchy level: the collagen fibrils.

In healthy tissue, collagen production is balanced by collagen degradation. The degradation of collagen is mediated in some cases by matrix metallo-proteinases (MMPs), enzymes that bind and cleave the triple helical tropocollagen molecule. If the balance between collagen production and degradation is disrupted, many disease states emerge, including post traumatic remodeling, arthritis, cancer, and fibrosis (Malemud, 2006; Mancini and Di Battista, 2006; Cawston and Wilson, 2006; Clark, 2008; Giannandrea and Parks, 2014). Understanding the connection between collagen degradation and the associated change in mechanical properties of collagen at the tissue level may lead to the development of tissue remodeling therapies for different pathologies.

During the last decade, improvement in experimental techniques allowed for a broader understanding of the effect of collagen degradation on the basic mechanics at the tissues level (Park, 2008; Laasanen, 2003; Panwar, 2013, 2015). For example, using a bovine knee articular cartilage, Laasanen and colleagues reported up to 70% reduction in the tissue's static elastic modulus after a chronic exposure to collagenase type IV (MMP) (Laasanen, 2003). Consistent results have also been observed by Park and collaborators who reported near 60% enzyme-mediated reduction in the equilibrium elastic modulus of bovine articular cartilage (Park, 2008).

At the fiber level, Panwar (2013, 2015) explored the effect of degradation on the mechanical properties of tendon collagen fibers using the mice tail. In these examinations, a cathepsin K (a cysteine protease) was employed to degrade the collagen fibrils. A significant reduction of the elastic modulus (~ 60%) and the associated ultimate stress at rupture was observed (Panwar, 2013). Using data from tissue and fiber

* Corresponding author at: Biomedical Engineering Department, Northwestern University, 2145 Sheridan Road, Evanston, IL 60208, USA.
*E-mail address:* y-dhaher@northwestern.edu (Y. Dhaher).

http://dx.doi.org/10.1016/j.jmbbm.2017.08.020
Received 11 March 2017; Received in revised form 10 August 2017; Accepted 15 August 2017
Available online 19 August 2017

level experiments, phenomenological models have been developed to describe the aggregate effect of enzyme-mediated changes on tissues mechanics. Unfortunately, these mathematical description of degradation does not take in account the molecular complexity of collagen degradation (Hadi et al., 2012; Hadi, 2012; Billiar and Sacks, 2000; Boerboom, 2003). While a connection between molecular structure and mechanical properties have been drawn in some experimental studies (Panwar, 2013, 2015), a comprehensive connection between structural changes (due to degradation) and the mechanical properties of collagen fibrils remains elusive.

Computational models offer an advantage since they can link molecular details to macroscopic behavior under the normal and degraded states. The majority of the computational approaches focus on the development of simulation constructs either at the nano-scale (tropocollagen level) (Chang and Buehler, 2014; Chang et al., 2012; Lu and Stultz, 2013; Perumal et al., 2008; Zhou et al., 2015; Pradhan et al., 2011) or meso-scale (fibril or fiber level) (Buehler, 2008a, 2008b, 2006a, 2011; Chang, 2012; Depalle, 2015, 2016) mechanics. For example, Pradhan et al. (2011) performed *all atomistic* steered molecular dynamics to investigated the effect of strain rate in a ~ 300 nm tropocollagen molecule. Zhou and colleagues employed a similar computational construct to investigate the mechanical properties derived from the gap and overlap structure of the micro-fibril (Zhou et al., 2015). While *all atomistic* models provide a detailed understanding of the mechanisms at the molecular level, extension of the approach to explore the connectivity to changes in mechanics at the fiber or tissue levels is computationally prohibitive. To this end, coarse grain approximations have been proposed. Buehler and colleagues (Chang and Buehler, 2014; Chang et al., 2012; Buehler, 2008a, 2008b, 2006a, 2011; Chang, 2012; Depalle, 2015; Gautieri, 2012a, 2012b, 2014; Uzel and Buehler, 2011) illustrated that the coarse graining approach (informed by data derived form atomistic simulations (Buehler, 2006b)) can yield significant insights into the basic mechanics at the fibril level. While most of these examinations focused on a 2-dimensional realization of the structure, in a recent study, Buehler and colleagues introduced a 3-dimensional representation of a collagen fibril focusing on the effect of enzymatic crosslink and mineralization processes on the mechanical properties (Depalle, 2015, 2016). In terms of computational models of degradation at the tropocollagen level, there are several molecular dynamics based simulations that analyze the interaction between MMPs and tropocollagen (Chang and Buehler, 2014; Chang et al., 2012; Lu and Stultz, 2013; Perumal et al., 2008). While informative, models that connect these molecular dynamic based results to the basic mechanics at the fibril or fiber are lacking.

In the present study, we seek to emulate the effect of fibril degradation (regardless of the origin) on the basic mechanics of the fibril. An implicit representation of the water was incorporated in the molecular simulations as a Langevin dynamics of the tropocollagen chains. We observed that surface degradation produce dramatic changes in the toughness of the collagen fibril, consistently with experimental observations (Park, 2008; Laasanen, 2003; Panwar, 2013, 2015). This aligns with the hypothesis that the molecular organization of the fibril plays a key role in the mechanical properties (Fratzl, 2008) and a small disruption of this structure leads to a high reduction of the fibril toughness. We also compare the effect of degradation and amount of enzymatic crosslink, tracing a comparison (verification) with previous works focused on enzymatic crosslink (Depalle, 2015). Finally, in order to understand the molecular mechanisms responsible for mechanical behavior, we calculated the distribution of tropocollagen bond lengths. Tropocollagen bond length distribution provides ways to quantify the stress distribution inside the fibril since more stretched bonds are experiencing more stress. In overall we present a comprehensive study of the effect of structural changes in collagen (due to degradation) and the mechanical response at the fibril level.

**Table 1**
Model parameters.

| Model parameters | Value |
|---|---|
| ε – Lennar Jones [Kcal/mol] | 6.87 |
| σ – Lennar Jones [Å] | 14.72 |
| $\theta_0$ – Equilibrium bending angle [degrees] | 180 |
| $k_\theta$ – Bending strength constant [Kcal/mol rad] | 14.98 |
| $r_0$ – Equilibrium distance (tropocollagen) [Å] | 14.00 |
| $r_1$ – Critical hypereslastic distance (tropocollagen) [Å] | 18.20 |
| $r_{break}$ – Bond breaking distance (tropocollagen) [Å] | 21.00 |
| $k_{T0}$ – Stretching strength constant (tropocollagen) [Å] | 17.13 |
| $k_{T1}$– Stretching strength constant (tropocollagen) [Å] | 97.66 |
| $r_0$ – Equilibrium distance (divalent crosslink) [Å] | 10.00 |
| $r_1$ – Critical hypereslastic distance (divalent crosslink) [Å] | 12.00 |
| $r_{break}$ – Bond breaking distance (divalent crosslink) [Å] | 14.68 |
| $k_{T0}$ – Stretching strength constant (divalent crosslink) [Å] | 0.20 |
| $k_{T1}$ – Stretching strength constant (divalent crosslink) [Å] | 41.84 |
| $r_0$ – Equilibrium distance (trivalent crosslink) [Å] | 8.60 |
| $r_1$ – Critical hypereslastic distance (trivalent crosslink) [Å] | 12.20 |
| $r_{break}$ – Bond breaking distance (trivalent crosslink) [Å] | 14.89 |
| $k_{T0}$ – Stretching strength constant (trivalent crosslink) [Å] | 0.20 |
| $k_{T1}$ – Stretching strength constant (trivalent crosslink) [Å] | 54.60 |
| m – mass tropocollagen beads [a.m.u] | 1358.7 |

## 2. Methods

### 2.1. Coarse grained model

We implemented a collagen type I coarse grained model based on parameters published in several reports by Buehler and colleagues (Buehler, 2008a, 2008b, 2006a, 2011; Depalle, 2015) and more precisely using the set of parameters developed for a 3-D representation of the model (Depalle, 2015, 2016). The parameters for the interaction potentials are given in Table 1. Tropocollagen is represented by a polymeric chain that contains 215 bonded beads units. A total 285 tropocollagen chains interact through a Lennard-Jones potential acting as the cohesive and repulsive force that keep the fibril together and prevent the interpenetration of beads, respectively. The potential is represented by the standard equation:

$$U_{LJ} = 4\epsilon\left[\left(\frac{\sigma}{r_{LJ}}\right)^{12} - \left(\frac{\sigma}{r_{LJ}}\right)^{6}\right] \quad (1)$$

where $U_{LJ}$ is the potential energy due to the interaction between two tropocollagen beads i and j, $r_{LJ}$ distance apart. The parameter ε represents the strength of the potential and σ is related to the position of the minimum in potential energy.

The bending angle between beads is controlled by a harmonic potential with the following equation:

$$U_\theta = k_\theta(\theta - \theta_0)^2 \quad (2)$$

where $U_\theta$ is the potential energy of the bending angle between three consecutively bonded tropocollagen beads i, j and k forming an angle θ. The parameter $k_\theta$ represent the bending strength in energy units and $\theta_0$ is the equilibrium angle.

The hyper-elastic bond (stretching) between tropocollagen beads is represented by 3-regime potential energy with a gradient defined by:

$$F_{bond} = \frac{\partial U_{bond}}{\partial r} = \begin{cases} k_{T0}(r - r_0) & if\ r < r_1 \\ k_{T1}(r - r_0) & if\ r_1 \le r < r_{break} \\ 0 & if\ r > r_{break} \end{cases} \quad (3)$$

where $r_0$ is the equilibrium distance between the two beads, $k_{T0}$ and $k_{T1}$ are the spring constants acting at different distances between 0 to $r_1$ and $r_1$ to $r_{break}$, respectively. Note that the gradient of the potential energy represents the force of interactions between two given beads.

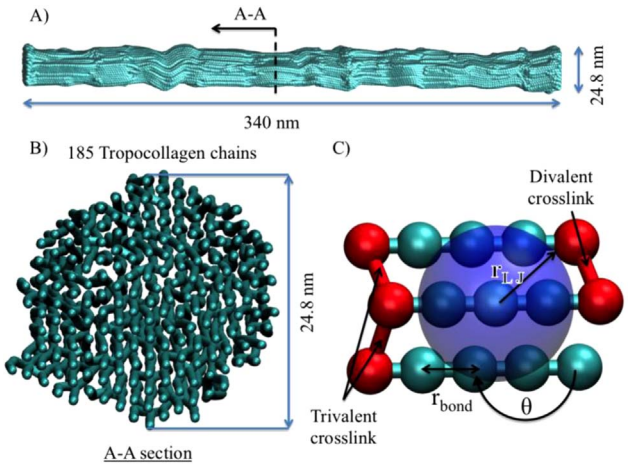


**Fig. 1.** Collagen fibril model. A) Transversal view of the fibril. B) Cross-section AA of the fibril. C) Diagram of bonded and non-bonded interactions.

### 2.2. Fibril structure

The morphology of our fibril model follows the experimentally observed fibrillar structure (Orgel, 2006). We built our initial fibrillar structure by arranging microfibrils following the typical hexagonal pattern. This simplified representation of the micro fibrils did not include a change in direction between the overlap and gap regions (Orgel, 2006). Tropocollagen chains consisted of 215 interconnected coarse-grained beads (Fig. 1). The micro-fibril geometry of the model was built by an arrangement of 5 tropocollagen molecules to form an initial micro-fibril. By aligning a total of 37 micro-fibrils, a 340 nm axial length (Fig. 1**A**) and 24.8 nm diameter collagen fibril was constructed (Fig. 1**B**). Enzymatic crosslinks are included in the model as bond connections between the terminal ends of tropocollagen and the nearest bead from the neighboring tropocollagen. The fibril contained a mix of trivalent and divalent enzymatic crosslinks, 33% trivalent to 66% divalent crosslinks. Divalent crosslinks are defined as bonds with only one adjacent tropocollagen while the trivalent crosslinks are defined as bonds to two neighboring tropocollagen molecules (Fig. 1**C**). The ratio of divalent/trivalent crosslinks used in this model was informed by experimental findings on cartilage and tendon (Saito, 1997; Svensson, 2013). As we modify the total amount of crosslinks, the ratio of the trivalent to divalent crosslinks remained approximately the same. Finally, the current model does not account for interactions with other molecules (GAGs, AGEs and adjacent fibrils) and focuses primarily on the degradation at the fibril level. Our choice of this construct is driven primarily by experimental data reported for fibril properties (model parameters) obtain under isolated loading conditions (Svensson, 2013).

### 2.3. Simulated degradation and mechanical properties

In this study we defined three different scenarios: crosslink removal, surface degradation and volumetric degradation. In each scenario removal of beads and crosslink connections occur in an intact equilibrated fibril followed by a new equilibration step. If a tropocollagen bead is removed during degradation, all the connections including crosslinks are removed. However, in the cases of surface and volumetric degradation, the amount of crosslink remains above 94% due to the large number of cleavable (candidates for removal) sites. Crosslink removal was implemented to verify our simulations against the recent work by Buehler and colleagues (Depalle, 2015).

For the surface degradation, we implemented an algorithm that cleaves tropocollagen beads from the fibril surface, mimicking the aggregate effect of the MMP mediated degradation. Beads prone to degradation were identified using a solvent-accessible-surface-area calculation (SASA) algorithm (Connolly, 1983) with a probe radius of 2 nm on an equilibrated fibril. It is important to note that MMPs are voluminous enzymes that need enough available space to bind and cleave the collagen fibril. Thus, only tropocollagen beads with certain accessible surface ($> 3\ nm^2$) were included as probable candidates to be cleaved (removed). This value of accessible surface is arbitrary and was decided based on the bimodal shape of the distribution of accessible surface values. While, it has been shown that MMPs are more prone to cleave tropocollagen near the C-terminal (Perumal et al., 2008), at the fibril level, the regions prone to interaction with MMPs are more difficult to predict due steric impediment and surface crowding. Thus and due to the uncertainty of cleavable site locations at the fibril level, the cleaved sites were chosen at random. The effect of such an assumption requires a closer synthesis of the dynamics of MMPs adsorption, a process that is beyond the scope of this study.

Volumetric degradation of the fibril was implemented in a similar way to surface degradation, but without any restriction on surface accessibility. The removed beads can belong to any of the tropocollagen chains of the fibril across the entire volume. Volumetric degradation, as defined in this study, is not observed in nature. Nevertheless, exploring changes in the mechanical behavior of this type of degradation offers insights into the significance of the structural layout of the collagen fibrils.

In the crosslink removal algorithm, we produced a random removal of all possible enzymatic crosslinks in the fibril starting from 100% of crosslink up to 0% crosslink in increments of 20%. In this case, all tropocollagen beads remained intact and only crosslink connections were removed. In this study, crosslink removal was used to validate of model simulations against previous computational models and served as a theoretical comparison with the effect of the surface and volumetric degradation.

Finally, for the quantification of the stress-strain response to the fibril axial loading, the strain was computed by tracking the change in the size of the simulation box and the stress tensor was computed using the virial stress metric, both implemented in LAMMPS (Plimpton, 1995). The abrupt fracture of the fibril was prevented by imposing a constraint on the maximum velocity limit to avoid the collapse of the simulation at large strains. Furthermore, the yield point defined in this model is equivalent to the fracture point observed in experiments reported by Svensson and colleagues (Svensson, 2013). The residual stress observed in the plastic region occurs due to cohesive forces between tropocollagen, which maintain the fibril connected over the timescale of the simulation. We analyzed the strain distribution inside the fibril by calculating the tropocollagen bond length distributions. The distribution is calculated based on the bond pairs of the fibril structure at the different fibril bulk strain values. This distribution allows for the quantification of sliding and stretching of tropocollagen chains during the deformation of the fibril. We herein define bonds with minimal change in length from the equilibrated state during an aggregate fibril stretch as sliding bonds; a constant inter-bead distance during stretch.

### 2.4. Simulation parameters

All simulations were performed using LAMMPS molecular dynamics simulation package (Plimpton, 1995). A 0.01 ps time step was used and the equations of motion were integrated with a Langevin thermostat that account for the implicit representation of water. In all simulations, the drag coefficient was set at 1000 ps and the temperature at 310 K. A maximum velocity constraint was imposed to observe the breakage of the fibril without the collapse of the structure. The strains were applied in the axial direction with periodic boundary conditions.

### 2.5. Model verification

While bond characteristics in the current model were consistent with the only other three-dimensional model of collagen fibril that included a cross-link degradation construct reported by Depalle (2015),

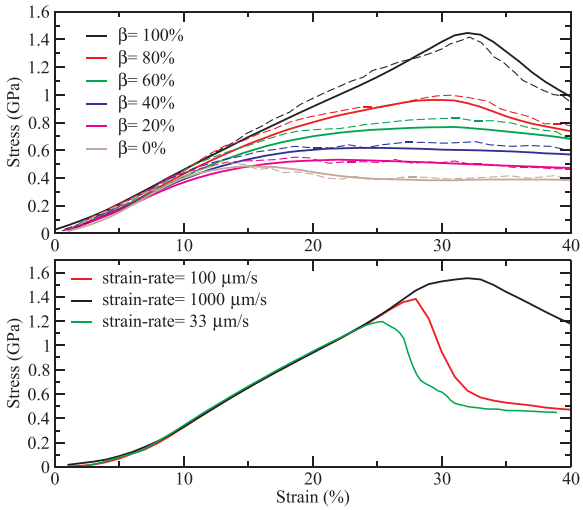


**Fig. 2.** (Top) Cross examination of simulation outputs of the current model (inclusion of divalent cross links only) against the only three-dimensional fibril model simulations reported in the literature with similar bond characteristics Ref. (Depalle, 2015). (Bottom) Stress-strain curve of the intact fibril including a mixture of di- and tri-valent bonds (100% crosslink and no degradation) at different strain rates. Unlike the Depalle model, the proposed model simulations included both the tri- and bi-valent connections. The different colors represent different strain rates; all the following calculations are made at 33 μm/s (green). (For interpretation of the references to color in this figure legend, the reader is referred to the web version of this article.)

differences remained in fibril morphology and simulation framework employed across models. A series of simulations were conducted with similar crosslink configuration as reported by Depalle et al. (only divalent cross-links accounted for) yielding consistent results (Fig. 2 **top panel**). The Langevin thermostat employed here seems to smooth the response of the strain-stress curves as shown in the figure. Small differences were observed highlighting the potential effects of differences in the initial structure (morphology) and the simulation parameters across the two models. Differences in the initial structure can be associated with changes in the stiffness of the fibril across models at the onset of the simulations. Morphologically, unlike in the Depalle et al. case, our initial structure did not include the change in direction between the overlap and gap region. We argue that the observed differences in the stress distribution between the two models may be attributed in part to the stress associated with the stretching of the kink located in this region. While small differences in simulation outputs were observed between the two models, the current model expressed consistent mechanical behavior observed in previous implementations of the parameters (Buehler, 2008a, 2008b, 2006a, 2011; Depalle, 2015, 2016) supporting a robust verification of the current model.

The strain rate used in the current simulations was 33 μm/s. To assess the robustness of the model to this assumption, simulations with faster strain rates were conducted and are shown in Fig. 2 (**bottom panel**). As shown, the pre yield behavior is not sensitive to the simulation strain rates. However, we observed that the location of the yield/fracture point is dependent on the strain rate used in the simulation. In this study, a strain rate of 33 μm/s was used because it was within the range of the experimental strain rates reported by Svensson (2013), a unique difference between the current and the Depalle et al. model.

### 2.6. Model comparison with experimental values

While a successful verification of the current model against prior computational efforts (Buehler, 2008a, 2006a, 2008b, 2011; Depalle, 2015) was achieved, cross examination of model simulation with experimental data was more complicated due to the computational constraints of implementing a fibril model with a morphology similar to the fibril sample used in experiments. For example, Svensson (2013) data

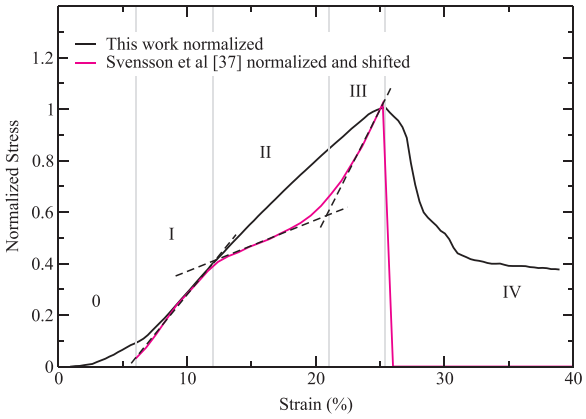


**Fig. 3.** Comparison of the normalized stress strain curve (100% crosslink – no degradation) for the current implementation of the model and normalized and shifted data from Svensson et al. (Saito, 1997). Dashed lines are used to help define the different elastic regions that are used in the following calculations.

was based on testing a fibril of ~ 33 μm in length and a ~ 100 nm in diameter. Our model consisted of a ~ 0.34 μm and a 24.8 nm fiber length and diameter, respectively. Moreover, key experimental information were not provided in the Svensson (2013) with the most critical of which is the level of pre-tensioning of the fibril sample. Fig. 3 illustrates the comparisons in the normalized stress-strain behavior between the current model and the experimental data (Svensson, 2013). Model simulations were conducted for the 100% crosslink and the no degradation version of the model. Different regions of the elastic regime were obtained based on the normalized experimental data observed in Fig. 3. This classification was based on the definition introduced in the literature (Depalle, 2015; Svensson, 2013), to understand the mechanical behavior of collagen fibril. These regions are not strictly well defined making the extrapolating these definitions post degradation difficult. Thus, in this paper we maintained the definition of the different regions based on an intact fibril as seen in Fig. 3. To account for the experimental pre-tension, the experimental values were shifted to match region I of the simulated results. The rationale behind shifting experimental values to match region I is that region 0 appears only in simulations without any pre-tension stress resulting in lower stress values for that region. While the computed and experimental mechanical responses had similar features (yield/fracture point, low strain elastic behavior), the model failed to capture the experimentally reported elastic behavior in regions II and III. The differences in these regions between the computed and experimental values are attributed in part to the model's parameterization of the crosslinks. We performed several non-exhaustive simulations to provide a mechanistic examination of the origin of these differences. We concluded that in order to match the slope in region II and region III with the experimental value, tropocollagen bond should have a shorter critical hyper-elastic distance and the trivalent bonds should have lower stiffness with a lower cohesive Lennard-Jones force. We also observed that differences in the post yield/fracture point are mostly due to residual stress associated with the cohesive Lennard-Jones force, since the fibril remain in close contact at the simulated strain range. An exhaustive parameter exploration study would have been computationally intractable requiring a significant and costly computational time-share on a super computer, a goal beyond the scope of this study and will be the target of future examinations with the experimentally matched morphology.

## 3. Results

Fig. 3 shows simulation results of the stress-strain behavior of an intact collagen fibril (100% crosslink and no degradation). The stress strain curve displays 5 characteristic regions as reported in prior experimental studies (Depalle, 2015; Svensson, 2013). The 5 regions of

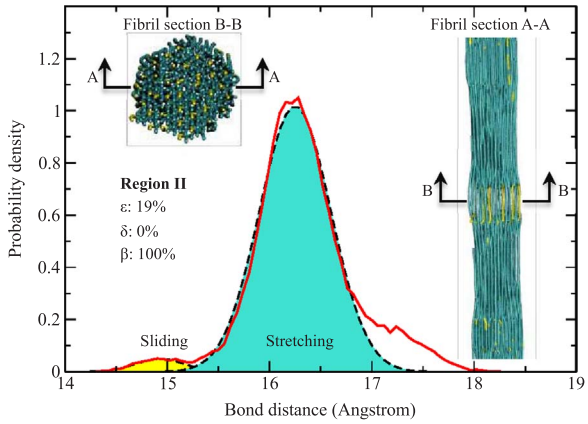


**Fig. 4.** Bond length distribution (solid red line) of an intact fibril (100% crosslink and no degradation) at 19% of strain. The dashed curves are Gaussian deconvolutions of the two main peaks Inset: diagram of the location of stretching/sliding bonds in the axial and frontal plane. (For interpretation of the references to color in this figure legend, the reader is referred to the web version of this article.)

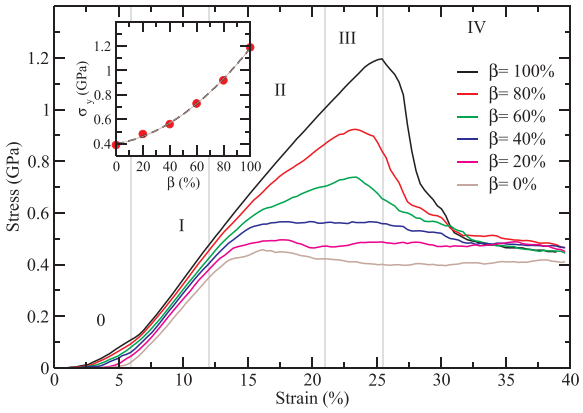


**Fig. 5.** Strain-stress curve as function of the amount of crosslink. Regions are based in a fibril with 100% crosslink. The dashed line indicates the shift in the yield point. Inset: Yield strength ($\sigma_y$) as a function of crosslink percent ($\beta$). Dashed line corresponds to a quadratic polynomial fit (Eq. (4)). (For interpretation of the references to color in this figure legend, the reader is referred to the web version of this article.)

the stress-strain response can be differentiated by their elastic behavior (dashed curves in Fig. 3 bottom). The goal of this study is to attempt to understand the effect of degradation (crosslink, surface and volumetric) on the behavior of these 5 regions of the stress-strain curve. In particular, we are going to focus on the response in region I, II and III with a special emphasis on region II (associated with the sliding of the tropocollagen chains). The distribution of the bond lengths will be computed to quantify the relative probability of sliding vs. stretching of the constituent tropocollagen chains for this region as a function of the degradation type.

Fig. 4 displays the bond length distribution of an intact fibril for the tropocollagen bonds (100% crosslink and no degradation) at 19% of strain (region II). As indicated in Table 1, the equilibrium tropocollagen bond distance is 14 Å, the transition to the hyper-elastic mode is at 18.2 Å and the bond break distance is 21 Å. The distribution of tropocollagen bond lengths in the intact fibril under axial stretch is dominated by bond lengths clustered around a ~ 16.2 Å. This peak represents a large population of tropocollagen bonds that experience similar stress as a response to the applied load. Upon closer examination the distribution shown two smaller population of bond lengths centered at ~ 14.8 Å and ~ 17.4 Å, respectively. The later represents bonds that are over stretched and are near the transition to the hyper-elastic mode. On the other hand, the ~ 14.8 Å cluster represents a population of tropocollagen bonds that are experiencing sliding with low bond stress levels, only 0.8 Å larger than the equilibrated bond length. The presence of three populations of bond lengths highlight the nonhomogeneous stretch and stress that the fibril undergoes during a simple axial loading boundary conditions. Moreover, as indicated by the fragments identified in yellow of the coarse grained representation inset in Fig. 4, bonds experiencing low level of stress or sliding motion seem to reside in the gap region of the D-band. The population of sliding bonds (peak at 14.8) and stretching bonds (peak at 16.2) are found by Gaussian deconvolution (dashed black lines). The use of a Gaussian deconvolution is only intended for qualitatively identification of the peaks.

### 3.1. Crosslink removal

As indicated earlier, prior computational work focused on understanding the role of enzymatic crosslink on the mechanical properties of collagen fibrils (Depalle, 2015). To qualitatively validate our model against prior work and to analyze the effect of crosslink removal in our model, we obtained the stress-strain response as a function of enzymatic crosslink (β) removal (Fig. 5). While the effect under a mixed divalent and trivalent crosslinks were not examined in prior work, our simulation results were consistent with earlier reports showing a decrease in the toughness (area under the curve) of the fibril following cross-link removal (Buehler, 2008a, 2006a, 2008b; Depalle, 2015).

One of the key features in the stress-strain response is that enzymatic crosslink removal produce no changes in the elastic behavior of region I. It has been proposed that this part of the stress-strain curve corresponds to the elasticity of the tropocollagen chains (Depalle, 2015; Svensson, 2013). Therefore, since the tropocollagen chains remain unbroken (at low strains) the elastic modulus of region I remains the same. Alternatively, region III, a region that depends on the elastic behavior of crosslinks (Depalle, 2015), a dramatic change was observed with the removal of crosslinks. We also observed that the crosslink removal produces a shift in the yield point toward lower strains (dashed line in Fig. 5). This change in the yield point is a consequence of removing crosslinks that interconnect tropocollagen chains. This change in the yield point is expressed in terms of a cross plot between the yield strength and percentage of crosslink as shown in the inset of the figure. The shift in the yield point as consequence of the crosslink removal can be expressed mathematically as follows (dashed line):

$$\sigma_y = \sigma^o_{y\beta} + 0.00186*\beta + 5.98*10^{-5}*\beta^2 \quad (4)$$

Where $\sigma_y$ is the yield strength, $\sigma^o_{y\beta}$ the yield strength of fiber with no crosslinks (0.39 GPa) and $\beta$is the percentage of crosslink removal. The minimal value of the yield strength computed in the absence of any cross-link ($\beta$ = 0%) represent the intermolecular forces associated with the Lennard-Jones potential.

Fig. 6 shows an illustrative tropocollagen bond length distribution of a fibril with a 60% crosslink, at 19% of strain (region II). As compared to the intact fiber (Fig. 4), the removal of crosslinks yielded an increase in the population of bonds experiencing low level of bond stresses. The nature of the inhomogeneity in stress has also been modified with the largest population of the stretched bonds. Informed by the axial and transverse cut shown in Fig. 6, a spatial representation of the sliding (yellow fragments) and stretching bonds is identified. The sliding appears along the fibril involving groups of near tropocollagen beyond those present in the D band observed during the axial loading of the intact fibril. This indicates that the underlying mechanism associated with the significant reduction in the yield strength (**Eq.** (4)) may be attributed to the effect of cross-link degradation in the sliding mechanics expressed in region II of the stress/strain response. The distribution of stress inside the fibril becomes less homogenous, and certain tropocollagen fibrils that remain connected account for the overall elasticity of the region II and III.

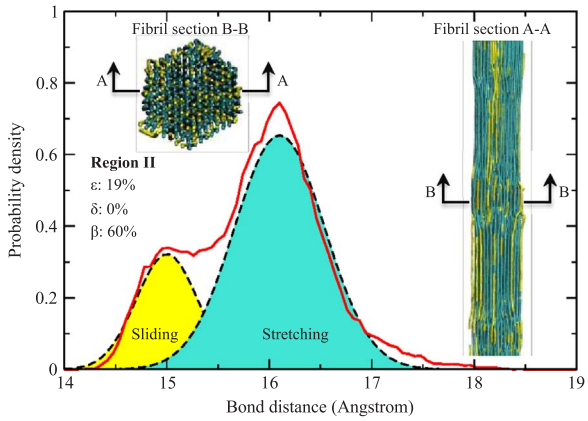


**Fig. 6.** Bond length distribution (solid red line) of a fibril with crosslink removal (60% crosslink) at 19% strain. The dashed curves are Gaussian deconvolutions of the two main peaks Inset: diagram of the location of stretching/sliding bonds in the axial and frontal plane. (For interpretation of the references to color in this figure legend, the reader is referred to the web version of this article.)

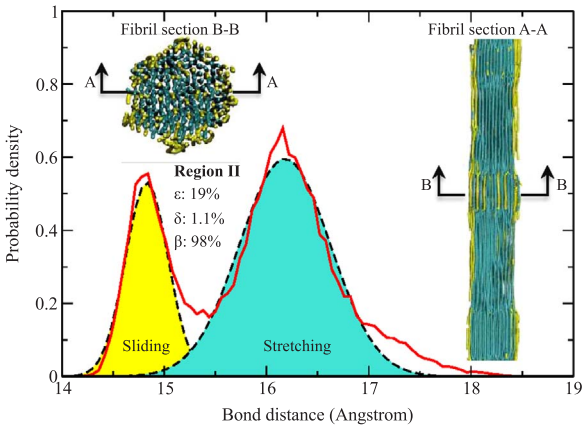


**Fig. 8.** Bond length distribution (solid red line) of a fibril with surface degradation (1.1% wt) at 19% strain. The dashed curves are Gaussian deconvolutions of the two main peaks Inset: diagram of the location of stretching/sliding bonds in the axial and frontal plane. (For interpretation of the references to color in this figure legend, the reader is referred to the web version of this article.)

### 3.2. Surface degradation

We have shown how modifying the enzymatic crosslinks change the mechanical response of the fibril. Now we want to investigate the effect of degradation δ on the mechanical properties of the fibril. In Fig. 7 we present stress-strain curves of a fibril at different levels of surface degradation. The percentage of surface degradation is the ratio between the removed bead and the total beads on the fibril (a percent weight of the fibril). The surface obtained by SASA is approximately 10% of the fibril weight. The main characteristics of degrading the surface are a decrease in elastic moduli, decrease in toughness and decrease in yield point of the fibril. Moreover, our simulations indicated that a small amount of surface degradation (i.e. 0.1% wt) yielded a numerically significant change in the basic mechanical properties of the fibril. On the other hand, these changes were minimal as the degradation increased beyond the 1.1%wt levels. This non-linear behavior is expressed in terms of a cross plot between the yield strength and percentage of degradation as shown in the inset of the figure. We can observe a rapid decay in the yield strength with a small amount of surface degradation (at 0.1% a reduction to ~ 86% of the intact yield strength) and a plateau type of behavior at high degradation (reduction to ~ 57% of the intact yield strength). The decay in yield strength as consequence of the surface degradation can be expressed mathematically by:

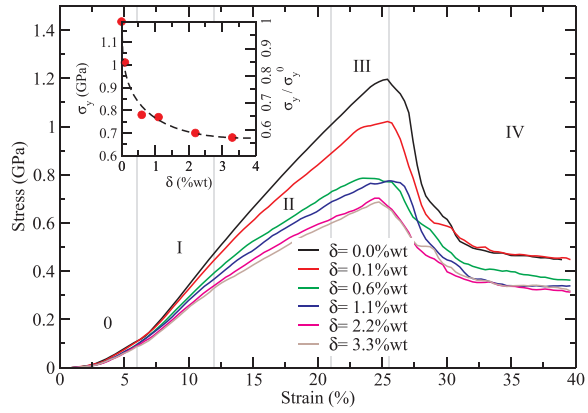


**Fig. 7.** Strain-stress curve as function of the amount of surface degradation. Regions are based in a un-degraded fibril with 100% crosslink. The dashed line indicates the shift in the yield point. Inset: Yield strength ($\sigma_y$) as a function of surface degradation ($\delta$). Dashed line corresponds to the fit in Eq. (5). (For interpretation of the references to color in this figure legend, the reader is referred to the web version of this article.)

$$\sigma_y = \sigma_y^o + 0.068*\delta - 0.503*\delta^{0.33} \quad (5)$$

where $\sigma_y$ is the yield stress, $\sigma_y^o$ the yield stress of the intact fiber (1.19 GPa) and $\delta$is the percentage of surface degradation in the fibril.

In addition, Fig. 7 indicates that the yield point, located approximately at the maximum stress point (~ 25.5% strain), remains at the same strain value for different degradation levels. This behavior arises from the fact that surface degradation is the combination of the properties of an intact fibril core and the decay of the properties of the external surface of the fibril.

Unlike in the crosslink removal case, surface degradation resulted in changes in regions I and III of the stress-strain curve (Fig. 7). The elastic modulus in region I (Mod 1) is approximately 0.68 GPa for an intact fibril and 0.49 GPa after a 3.3%wt surface degradation, equivalent to ~ 72% of reduction in Mod 1elastic modulus.

Fig. 8 shows the tropocollagen bond length distribution of a fibril with 1.1%wt, at 19% of strain (region II). As shown, the introduction of cleaved sites (removed of surface bonds) substantially changes the distribution of bond lengths. A clear bimodal distribution emerges with two distinct populations, stretching bonds (at ~ 16.2 Å) and sliding bonds (at ~ 14.8 Å). A significant increase in the number of sliding bonds when compared to the cross-link removal case (Fig. 6). The spatial locations of sliding (yellow) and stretching (cyan) bonds in axial and transversal sections of the fibril are shown. As indicated by the two representations, sliding bonds are mostly located on the surface for this degradation scheme and included sliding bonds the gap region of the intact core (consistent with the behavior of the intact fibril under axial loading). This indicates that cleaving tropocollagen bonds on the surface produce bonds that are irregularly connected (sliding bonds) and the load is mostly taken by the intact core.

In Fig. 9 we present the tropocollagen bond length distribution over the full range of strain values, a generalization of the special case given in Fig. 4. This figure provides an aggregate representation of bond distances across all four regions of the mechanical response of the intact fibril (top panel) and the 1.1% wt surface degraded fiber. For the intact fiber, region 0 (un-coiling of the fibril), the distribution is very narrow (identified by the red color), showing a high probability of bond length expressed around ~ 14.6 Å. The equilibrated bond length at zero strain is due to the initial strong cohesive Lennard-Jones potential. Region I display a color scheme that indicates a wider distribution of bond lengths, dominated by the stretching of tropocollagen chains. In Region II, the distribution becomes wider due to the presence of a population of sliding bonds (see Fig. 4 for an exemplar response at a given strain value). The Region III bond length distribution becomes increasingly wider and flat due to the sliding bonds, but also displays a population of

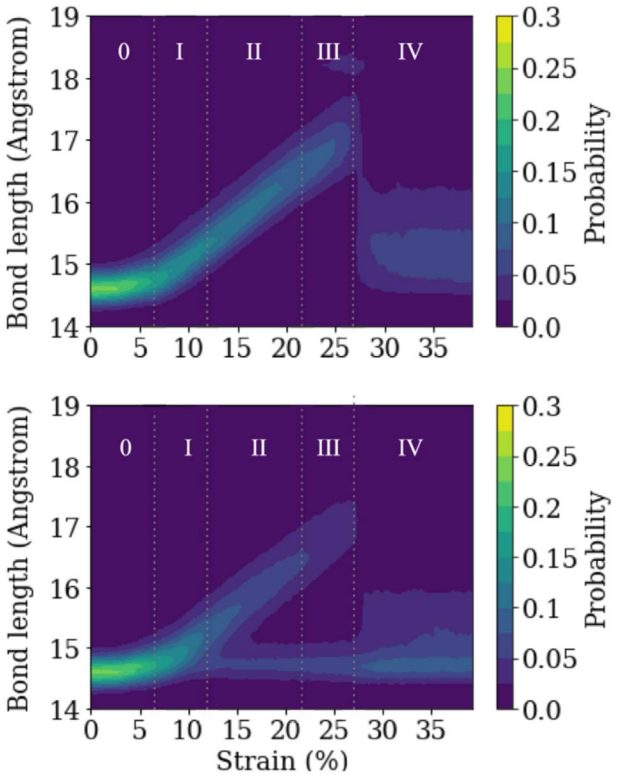


**Fig. 9.** Distribution of bond lengths as a function of the strain. Upper panel: Intact fibril (100% crosslink and 0% degradation). Lower panel: Surface degradation of 1.1%wt. (For interpretation of the references to color in this figure legend, the reader is referred to the web version of this article.)

overstretched bonds near the hyper-elastic region (~ 18.2 Å). Finally, region IV shows the yield of the fibril where a broad distribution of distances due to the residual stress emerges.

Fig. 9 lower panel displays the distribution of tropocollagen bond lengths as function of the strain for 1.1%wt of surface degradation. Mechanistically the fibrils experience complete different distributions of stress due to degradation. Qualitatively, the region representing the un-coiling of the fibril (region 0) maintained similar characteristics for both the intact and surface degraded fibrils. But region I clearly show the beginning of the differentiation between stretching and sliding bonds as a wide distribution of bond lengths are expressed. In regions II and III, the stretching and sliding bonds finally separate into a bimodal distribution that indicates the differential contribution of the degraded surface and intact core in resisting the applied load. Post yield (region IV) the distinction between the mechanical role of the core and surface bonds diminish, dominated by sliding bonds.

### 3.3. Volumetric degradation

As a qualifier and to test the hypothesis that the fibril core plays a significant role in maintaining the mechanical integrity under axial load pre yield, we observed that very low levels of volumetric degradation $\delta_v$ (0.1% wt) produce comparable change in the mechanical behavior as surface degradation (Fig. 10). But as the % degradation increase, the toughness of the fibril decrease abruptly (Fig. 10). This result is consistent with the notion that the structural morphology of the fibril is a key factor in maintaining its toughness (Fratzl, 2008). We can also observe that the shape of the stress-strain curve is progressively changing as we increase the degradation. Recall that in this study, volumetric degradation occurs in the entire fibril and it is likely that there is a critical % degradation that may have an adverse effect on the mechanical integrity of the fibril core. This difference in the degradation scheme between surface and volumetric degradation may explain the

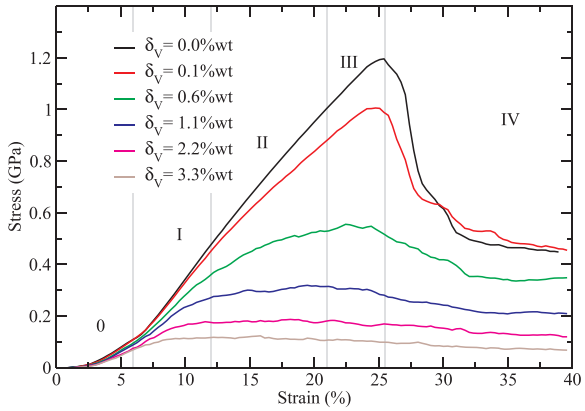


**Fig. 10.** Strain-stress curve as function of the amount of volumetric degradation. Regions are based in a un-degraded fibril with 100% crosslink. (For interpretation of the references to color in this figure legend, the reader is referred to the web version of this article.)

reason in the shift of the yield point towards lowers strains, in contrast with surface degradation were the yield point remains approximately constant. In addition, the volumetric degradation scheme resulted in a profound change in the computed elastic moduli representing the three regions, region I, II and III. In particular, region II and III elastic moduli seem to be more sensitive to the disruption of the fibril structure. Since the amount of crosslinks remains roughly above 90% during the random volumetric degradation, then the reduction of the toughness of region III (usually dominated by the crosslink strength) is mainly due to a facilitated sliding of tropocollagen.

To illustrate this, we show a tropocollagen bond length distribution of a fibril with 1.1%wt of volumetric degradation, at 19% of strain (region II), Fig. 11. It is clear that a comparable degradation per fibril weight employed across the whole volume leads unimodal distribution of boned lengths skewed to bonds experience sliding modes as compared to an equivalent surface degradation (Fig. 8). We can observe from the transversal cut that sliding bonds are located in the entire fibril. In a similar way, the axial cut displays sliding bonds located all along the fibril.

## 4. Discussion

We have shown that introducing defects in the molecular structure of collagen fibril (crosslink removal, surface degradation and volumetric degradation) produces dramatic reduction in its mechanical

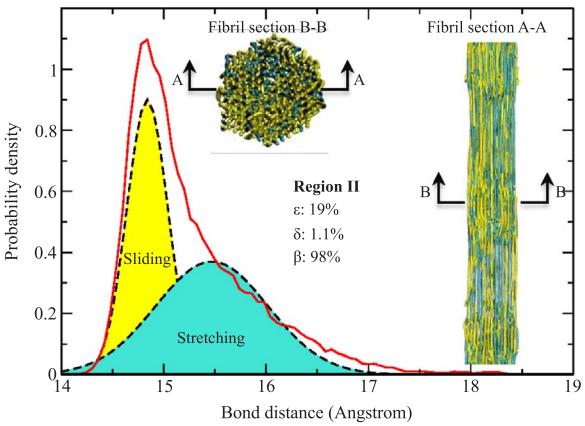


**Fig. 11.** Bond length distribution (solid red line) of a fibril with volumetric degradation (1.1%wt) at 19% strain. The dashed curves are Gaussian deconvolutions of the two main peaks. Inset: diagram of the location of stretching/sliding bonds in the axial and frontal plane. (For interpretation of the references to color in this figure legend, the reader is referred to the web version of this article.)

properties. A relatively small amount of defects is sufficient to yield a significant change in the mechanical behavior of the fibril. These findings are consistent with prior experimental observations showing a significant change in the mechanical property of the fibril due to modest exposure to MMP concentrations (Laasanen, 2003). In this paper, we also explored the differential effect of degradation type on the basic mechanics of the fibril. For enzymatic crosslink removal, the change in the mechanical properties is mostly due to changes in region II and III, a finding consistent with a prior computational report (Depalle, 2015). The reduction in crosslink favors the sliding of tropocollagen molecules and produces decay in the yield stress, shifting the yield point to lower strain values. On the other hand, we found that degradation on the surface of the fibril, emulating the MMPs action, substantially modified the fibril mechanics in region I, II and III of the stress-strain response with a significant decrease in the fibril yield stress as a function of % degradation. Our model indicated that while progressive decrease in yield stress as a function of degradation was present, the change in the yield stress plateaued at the 57% reduction from the intact fiber yield value. This result is qualitatively consistent with the experimental observations by Panwar (2013, 2015) reporting up to 57% steady state change in yield stress post cathepsin K treatment. Our pre-yield data on the degradation induced reduction in fibril modulus at steady state in region I is consistent with prior experimental reports (Park, 2008; Laasanen, 2003; Panwar, 2013, 2015), yielding a ~ 72% reduction in Mod 1 at high values of surface degradation.

To test the notion that the fibril core plays a significant role in maintaining the mechanical integrity under axial load pre yield, a volumetric degradation scheme was used. We found that the reduction in the mechanical properties is much more dramatic than with the surface degradation. While the elastic modulus of region I changed, the effect of volume degradation significantly affected the basic signature regions II and III. This is due to a facilitated sliding of the tropocollagen molecules induced by the presence of cleaved sites.

As previous simulations using this model have shown (Depalle, 2015) there is an overestimation of the elastic modulus in the low and large strain region (Mod. 1 and 2 respectively) in comparison with experimental findings (Svensson, 2013). This difference may be due to a combination of size effects, entropic effects and model parameterization errors. Nevertheless the model had proved to be robust and relievable in the prediction of mechanical properties of collagen fibrils (Buehler, 2008a, 2006a, 2008b, 2011; Depalle, 2015, 2016). Moreover, this is the first model that describes quantitatively enzymatic degradation and molecular mechanism at the fibril level.

## 5. Conclusion

In this work we have shown that introducing degradation in a collagen fibril produce dramatic non-linear decay in the mechanical properties of the fibril. We provide a quantitative understanding of the effect of cleave sites in the mechanical properties of a collagen fibril using a molecular dynamics coarse grain model. Moreover we provide a molecular structural model of the reduction in toughness due to sliding and stretching of tropocollagen chains. We also provide a parallel comparison with experimental work (that validate our model) and offer a framework that helps to understand the strain-stress curves due to degradation. Finally, this work also provides a theoretical framework for future multi-scale models of enzymatic degradation of tissue, since we provide a mathematical description of the decay in yield strength as a function of surface degradation.

## Acknowledgment

We would like to thanks Prof. M. J. Buehler and B. Depalle for the discussion in the implementation of the model. We also would like to thanks the support of the National Institute of Health through the grant # 4UOA1EB015410-04 and # 3U01EB015410-03S1.

## References

Billiar, K.L., Sacks, M.S., 2000. Biaxial mechanical properties of the native and glutaraldehyde-treated aortic valve cusp: Part II – a structural constitutive model. J. Biomech. Eng. 122 (4), 327–335.
Boerboom, R.A., et al., 2003. Finite element model of mechanically induced collagen fiber synthesis and degradation in the aortic valve. Ann. Biomed. Eng. 31 (9), 1040–1053.
Buehler, M.J., 2006a. Nature designs tough collagen: explaining the nanostructure of collagen fibrils. Proc. Natl. Acad. Sci. USA 103 (33), 12285–12290.
Buehler, M.J., 2006b. Atomistic and continuum modeling of mechanical properties of collagen: elasticity, fracture, and self-assembly. J. Mater. Res. 21 (8), 1947–1961.
Buehler, M.J., 2008a. Molecular architecture of collagen fibrils: a critical length scale for tough fibrils. Curr. Appl. Phys. 8 (3–4), 440–442.
Buehler, M.J., 2008b. Nanomechanics of collagen fibrils under varying cross-link densities: atomistic and continuum studies. J. Mech. Behav. Biomed. Mater. 1 (1), 59–67.
Buehler, M.J., 2011. Atomistic and continuum modeling of mechanical properties of collagen: elasticity, fracture, and self-assembly. J. Mater. Res. 21 (08), 1947–1961.
Cawston, T.E., Wilson, A.J., 2006. Understanding the role of tissue degrading enzymes and their inhibitors in development and disease. Best Pract. Res. Clin. Rheumatol. 20 (5), 983–1002.
Chang, S.W., et al., 2012. Molecular mechanism of force induced stabilization of collagen against enzymatic breakdown. Biomaterials 33 (15), 3852–3859.
Chang, S.W., Shefelbine, S.J., Buehler, M.J., 2012. Structural and mechanical differences between collagen homo- and heterotrimers: relevance for the molecular origin of brittle bone disease. Biophys. J. 102 (3), 640–648.
Chang, S.-W., Buehler, M.J., 2014. Molecular biomechanics of collagen molecules. Mater. Today 17 (2), 70–76.
Clark, I.M., et al., 2008. The regulation of matrix metalloproteinases and their inhibitors. Int. J. Biochem. Cell Biol. 40 (6–7), 1362–1378.
Connolly, M.L., 1983. Solvent-accessible surfaces of proteins and nucleic acids. Science 221 (4612), 709–713.
Depalle, B., et al., 2015. Influence of cross-link structure, density and mechanical properties in the mesoscale deformation mechanisms of collagen fibrils. J. Mech. Behav. Biomed. Mater. 52, 1–13.
Depalle, B., et al., 2016. Large deformation mechanisms, plasticity, and failure of an individual collagen fibril with different mineral content. J. Bone Miner. Res. 31 (2), 380–390.
Fratzl, P., 2008. Collagen Structure and Mechanics. Springer, US.
Gautieri, A., et al., 2012a. Hydration and distance dependence of intermolecular shearing between collagen molecules in a model microfibril. J. Biomech. 45 (12), 2079–2083.
Gautieri, A., et al., 2012b. Viscoelastic properties of model segments of collagen molecules. Matrix Biol. 31 (2), 141–149.
Gautieri, A., et al., 2014. Age- and diabetes-related nonenzymatic crosslinks in collagen fibrils: candidate amino acids involved in advanced glycation end-products. Matrix Biol. 34, 89–95.
Giannandrea, M., Parks, W.C., 2014. Diverse functions of matrix metalloproteinases during fibrosis. Dis. Model Mech. 7 (2), 193–203.
Hadi, M.F., et al., 2012. Simulated remodeling of loaded collagen networks via strain-dependent enzymatic degradation and constant-rate fiber growth. Mech. Mater. 44, 72–82.
Hadi, M.F., Sander, E.A., Barocas, V.H., 2012. Multiscale model predicts tissue-level failure from collagen fiber-level damage. J. Biomech. Eng. 134 (9), 091005.
Hulmes, D.J., 2002. Building collagen molecules, fibrils, and suprafibrillar structures. J. Struct. Biol. 137 (1–2), 2–10.
Laasanen, M.S., et al., 2003. Biomechanical properties of knee articular cartilage. Biorheology 40 (1–3), 133–140.
Lu, K.G., Stultz, C.M., 2013. Insight into the degradation of type-I collagen fibrils by MMP-8. J. Mol. Biol. 425 (10), 1815–1825.
Malemud, C.J., 2006. Matrix metalloproteinases (MMPs) in health and disease: an overview. Front. Biosci. 11, 1696–1701.
Mancini, A., Di Battista, J.A., 2006. Transcriptional regulation of matrix metalloprotease gene expression in health and disease. Front. Biosci. 11, 423–446.
Orgel, J.P., et al., 2006. Microfibrillar structure of type I collagen in situ. Proc. Natl. Acad. Sci. USA 103 (24), 9001–9005.
Panwar, P., et al., 2013. Effects of cysteine proteases on the structural and mechanical properties of collagen fibers. J. Biol. Chem. 288 (8), 5940–5950.
Panwar, P., et al., 2015. Changes in structural-mechanical properties and degradability of collagen during aging-associated modifications. J. Biol. Chem. 290 (38), 23291–23306.
Park, S., et al., 2008. Cartilage mechanical response under dynamic compression at physiological stress levels following collagenase digestion. Ann. Biomed. Eng. 36 (3), 425–434.
Perumal, S., Antipova, O., Orgel, J.P., 2008. Collagen fibril architecture, domain organization, and triple-helical conformation govern its proteolysis. Proc. Natl. Acad. Sci. USA 105 (8), 2824–2829.
Plimpton, S., 1995. Fast parallel algorithms for short-range molecular dynamics. J. Comput. Phys. 117 (1), 1–19.
Pradhan, S.M., Katti, D.R., Katti, K.S., 2011. Steered molecular dynamics study of mechanical response of full length and short collagen molecules. J. Nanomech. Micromech. 1 (3), 104–110.
Prockop, D.J., Kivirikko, K.I., 1995. Collagens - molecular-biology, diseases, and potentials for therapy. Annu. Rev. Biochem. 64, 403–434.
Saito, M., et al., 1997. Single-column high-performance liquid chromatographic-fluorescence detection of immature, mature, and senescent cross-links of collagen. Anal. Biochem. 253 (1), 26–32.

Shoulders, M.D., Raines, R.T., 2009. Collagen structure and stability. Annu. Rev. Biochem. 78, 929–958.
Svensson, R.B., et al., 2013. Fracture mechanics of collagen fibrils: influence of natural cross-links. Biophys. J. 104 (11), 2476–2484.
Uzel, S.G., Buehler, M.J., 2011. Molecular structure, mechanical behavior and failure mechanism of the C-terminal cross-link domain in type I collagen. J. Mech. Behav. Biomed. Mater. 4 (2), 153–161.
Zhou, Z., Minary-Jolandan, M., Qian, D., 2015. A simulation study on the significant nanomechanical heterogeneous properties of collagen. Biomech. Model Mechanobiol. 14 (3), 445–457.